Pressure dependent stability and structure of carbon dioxide—A density functional study including long-range corrections

Sebastian Gohr, Stefan Grimme, Tilo Söhnel, Beate Paulus, and Peter Schwerdtfeger

Citation: The Journal of Chemical Physics **139**, 174501 (2013); doi: 10.1063/1.4826929
View online: http://dx.doi.org/10.1063/1.4826929
View Table of Contents: http://scitation.aip.org/content/aip/journal/jcp/139/17?ver=pdfcov
Published by the AIP Publishing

Pressure dependent stability and structure of carbon dioxide—A density functional study including long-range corrections

Sebastian Gohr,[1,a)] Stefan Grimme,[2,b)] Tilo Söhnel,[3,c)] Beate Paulus,[1,d)] and Peter Schwerdtfeger[4,e)]

[1]*Institut für Chemie und Biochemie, Physikalische und Theoretische Chemie, Freie Universität Berlin, Takustr. 3, D-14195 Berlin, Germany*
[2]*Mulliken Center for Theoretical Chemistry, Institute for Physical and Theoretical Chemistry, Beringstr. 4, D-53115 Bonn, Germany*
[3]*Department of Chemistry, University of Auckland, Private Bag 92019, Auckland, New Zealand*
[4]*Centre for Theoretical Chemistry and Physics, The New Zealand Institute for Advanced Study, Massey University Auckland, 0745 Auckland, New Zealand and Fachbereich Chemie, Philipps-Universität Marburg, Hans-Meerwein-Str., D-35032 Marburg, Germany*

(Received 3 August 2013; accepted 11 October 2013; published online 4 November 2013)

First-principles density functional theory (DFT) is used to study the solid-state modifications of carbon dioxide up to pressures of 60 GPa. All known molecular CO_2 structures are investigated in this pressure range, as well as three non-molecular modifications. To account for long-range van der Waals interactions, the dispersion corrected DFT method developed by Grimme and co-workers (DFT-D3) is applied. We find that the DFT-D3 method substantially improves the results compared to the uncorrected DFT methods for the molecular carbon dioxide crystals. Enthalpies at 0 K and cohesive energies support only one possibility of the available experimental solutions for the structure of phase IV: the $R\bar{3}c$ modification, proposed by Datchi and co-workers [Phys. Rev. Lett. **103**, 185701 (2009)]. Furthermore, comparing bulk moduli with experimental values, we cannot reproduce the quite large—rather typical for covalent crystal structures—experimental values for the molecular phases II and III. © *2013 AIP Publishing LLC*. [http://dx.doi.org/10.1063/1.4826929]

I. INTRODUCTION

To accurately simulate phase diagrams up to a high temperature and pressure range by quantum theoretical methods is currently a formidable task.[1] Moreover, for molecular crystals, dispersive-type of forces need to be included to obtain reasonable structures and properties up to pressures where the repulsive wall becomes dominant. CO_2 is a molecular crystal with a rather small electric dipole polarizability (17.54 a.u.)[2,3] but a sizable electric quadrupole moment (−3.19 a.u.)[2,4] compared to other molecules,[5] i.e., in the bonding region and at long range the interaction between two CO_2 molecules is dominated by dispersive (van der Waals) and electrostatic quadrupole interactions.[6] This results in a rather small interaction energy between two CO_2 molecules, which is estimated to be 5.8 kJ/mol,[6] with a next-neighbor C–C distance of 3.602 Å,[7] which increases to around 26 kJ/mol[8,9] for the molecular crystal, but interestingly with a substantially increased next-neighbor C–C distance of 3.885 Å.[10] These rather small interaction energies explain the rather low CO_2 liquid-to-gas and solid-to-liquid phase transition temperatures of 216.6 K and 194.7 K, respectively. However, unlike the rare gases, where an expansion into many-body interaction potentials is relatively straightforward and can be used up to high-pressures,[11] such interaction potentials require a higher-dimensional treatment for the two- (and three-body) forces similar to water.[12,13] It is therefore perhaps more convenient to directly obtain the interaction energies between CO_2 molecules in the solid or liquid phase from accurate quantum theoretical methods.

The treatment of molecular crystals using accurate wavefunction based theory is however far from being trivial.[16,17] Even though great progress has been made in the past decade in the accurate treatment of solids using path-integral quantum Monte Carlo techniques,[18,19] random-phase approximations,[20] or incremental coupled-cluster schemes,[21] these methods are currently computationally too demanding to treat the equation of state (EOS) for molecular solids such as CO_2 for a large temperature-pressure range as shown in Figure 1. Density functional theory (DFT) is computationally more efficient but suffers from the fact that it is difficult to systematically improve the approximations such that convergence towards experimental values is achieved.[22] Recent improvements in the treatment of dispersive-type of interaction within DFT, however, opens up the treatment of molecular crystals such as bulk CO_2.[23–25] Subsequent test calculations on weakly interacting molecular systems (including the CO_2 dimer) gave very encouraging results.[26–28]

CO_2 is a potent green-house gas and a detailed understanding of the equation of state for CO_2 is important for future CO_2 storage and separation from other gases.[29] To get a first impression, Figure 1 presents an illustration of the

[a)]sebastian.gohr@tu-berlin.de
[b)]grimme@thch.uni-bonn.de
[c)]t.soehnel@auckland.ac.nz
[d)]b.paulus@fu-berlin.de
[e)]Author to whom correspondence should be addressed. Electronic mail: p.a.schwerdtfeger@massey.ac.nz

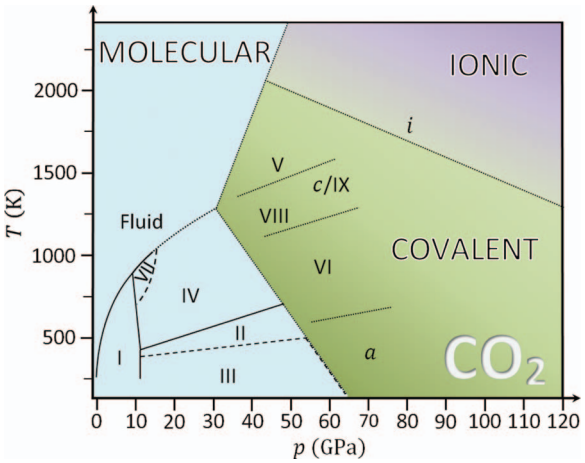

FIG. 1. (p, T)-phase diagram for carbon dioxide. The dashed lines are proposed to be kinetic transition barriers and the dotted lines are assumed (mostly hypothetical) phase transition lines. The information were taken from Refs. 14 and 15. "*a*" denotes the amorphous phase, "*c*" the coesite-like phase IX, and "*i*" the ionic modification.

phase diagram (similar illustrations can be found, e.g., in Refs. 30–32). Most of the drawn phase boundaries are not as well-known as the picture might suggest. In fact only the boundaries between the phases I and IV and I and VII could be measured with a high accuracy.[33] Furthermore, the three latest non-molecular modifications (phases VIII,[34] IX,[35] and an ionic modification[15]) have only been found by one group so far and are not yet confirmed by other studies. Apart from a controversy about the structure of phase IV,[32,36] there are also unsolved conflicts between experimental and theoretical structures, as for example between the two proposed experimental solutions for phase II[37] and the theoretical investigations by Bonev *et al.*[30] Another field of debate is the long-lasting discussion on phase V (see, e.g., Refs. 38–42). Also the correct structure of phase VI is not known so far, even though various possible modifications have been investigated theoretically,[43–45] none of these structures could produce an exact match for the experimental X-ray diffraction pattern from Ref. 46. While molecular dynamics simulations starting from phase III resulted in a covalent non-layered $P4_12_12$ structure,[44] the layered modifications are favored in all the above mentioned theoretical investigations on phase VI. Besides this observation, we included the covalent $P4_12_12$ structure in our work to see if we can reproduce this finding.

Already ten years ago, Bonev and co-workers published a theoretical investigation, in which they calculated the CO_2 phase diagram for three different phases of carbon dioxide ($Pa\bar{3}$, *Cmca*, and $P4_2/mnm$) using the standard PBE functional by Perdew, Burke, and Ernzerhof.[30] Here we investigate ten different solid-state modifications – which are shown in Figure 2 – using various dispersion corrected density functionals to estimate the importance of weak intermolecular interactions in the low to intermediate pressure range. For this we use the newly developed method by Grimme and co-workers,[23–25,47] and show that the inclusion of such effects is required to achieve results in good agreement with experimental data.

II. COMPUTATIONAL DETAILS

The solid-state structures of CO_2 as shown in Figure 2 were investigated using the following density functionals: the local density functional approximation (LDA),[51,52] the Perdew-Burke-Ernzerhof gradient corrected (GGA) functional (PBE),[53,54] the GGA functional of Perdew and Wang (PW91),[55,56] and the PBEsol (PBE revised for solids by Perdew and co-workers)[57] functional as implemented in the "Vienna *ab initio* simulation package" (VASP).[58–61] We adopted the plane-wave projector augmented wave method (PAW) by Blöchl[62,63] with a plane-wave energy cutoff of 700 eV and a $5 \times 5 \times 5$ k-point grid. In order to account for long-range corrections (LRC) of intermolecular interactions, especially for the molecular crystals in the low-pressure range, we applied the London dispersion two-body correction to the DFT approximation (DFT-D3) developed by Grimme and co-workers,[24] and the older PBE-D2[64] method for comparison, i.e., the following expression for the electronic energy is used:

$$E_{\mathrm{LRC}}^{\mathrm{DFT}} = E^{\mathrm{DFT}} + E_{\mathrm{disp}}^{\mathrm{APW}}, \tag{1}$$

with the atomic pair-wise dispersion correction

$$E_{\mathrm{disp}}^{\mathrm{APW}} = -\sum_{A<B}\sum_{n=6,8,10,\ldots} s_n \frac{C_n^{AB}}{R_{AB}^n} f_{\mathrm{damp}}(R_{AB}), \tag{2}$$

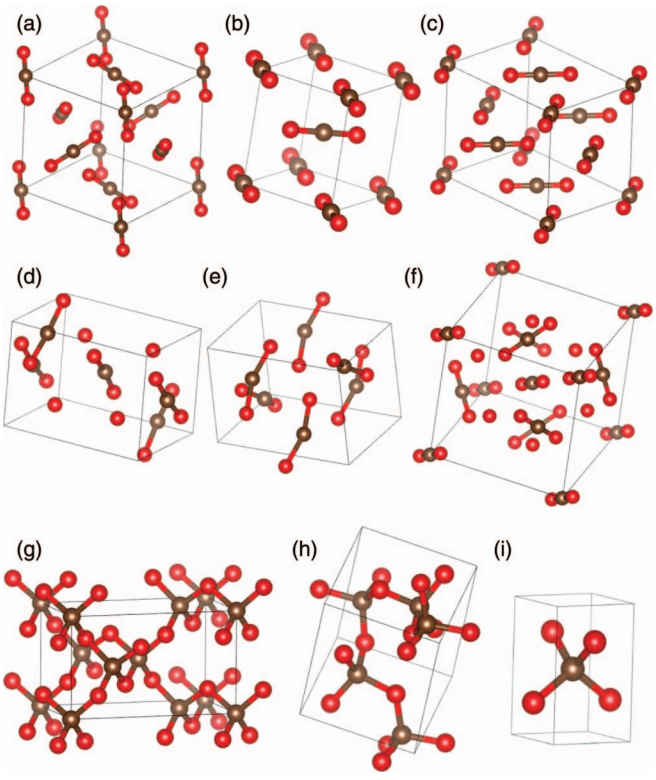

FIG. 2. Experimental (a)–(g) and theoretically predicted [(h) and (i)] structures for the investigated carbon dioxide phases. Brown colored atoms signify carbon, red atoms oxygen. (a) Phase I-$Pa\bar{3}$;[10] (b) phase II-$P4_2/mnm$ and phase II-*Pnnm*[37] (both structures are only slightly different); (c) phase III-*Cmca*[48] and phase VII-*Cmca*[49] (both structures are only slightly different); (d) phase IV-$P4_12_12$;[50] (e) phase IV-*Pbcn*;[50] (f) phase IV-$R\bar{3}c$;[14] (g) phase V-$I\bar{4}2d$;[41,42] (h) non-molecular modification $P4_12_12$;[44] (i) phase VI-$P\bar{4}m2$.[44]

s_n is a scaling factor which can conveniently be adjusted to correct for the repulsive behavior of the exchange-correlation functional chosen.[24] While DFT-D2 only uses fixed values of van der Waals dispersion coefficients C_6^{AA} and obtains C_6^{AB} ($A \neq B$) through a geometric mean, the more advanced DFT-D3 method uses the Casimir–Polder relation to obtain all necessary C_6^{AB} coefficients. The damping function is chosen such that $f_{\text{damp}}(R_{AB})/R_{AB}^n$ becomes very small for distances R_{AB} much smaller than the van der Waals radii of the two atoms A and B (zero damping, ZD), e.g.,

$$f_{\text{damp}}^{\text{ZD}}(R_{AB}) = (1 + e^{-\gamma(R_{AB}/(a_n R_{AB}^0)-1)})^{-1}. \quad (3)$$

As was pointed out by Grimme and co-workers, however, the correct dispersion interaction approaches a finite value at zero interatomic distances, and one may therefore prefer a Becke–Johnson (BJD) type of damping function,[65]

$$E_{\text{disp}}^{\text{APW}} = -\sum_{A<B}\sum_{n=6,8,10,\ldots} s_n \frac{C_n^{AB}}{R_{AB}^n + \left[f_{\text{damp}}(R_{AB}^0)\right]^n}, \quad (4)$$

with

$$f_{\text{damp}}^{\text{BJD}}\left(R_{AB}^0\right) = a_1 R_{AB}^0 + a_2. \quad (5)$$

In addition, Grimme pointed out that BJD is slightly superior over the ZD method. In order to investigate such effects for solid CO_2, we used both damping functions within the PBE-D3 approximation, while for PW91 and PBEsol only BJD was applied. In accordance with the recommendation from Ref. 24, only pair-wise dispersion corrections were applied. For the pair-wise dispersion interaction between the CO_2 molecules, we used the van der Waals coefficients C_6 and C_8 only. All adjustable parameters used can be found in Refs. 24, 64, and 66. Since there was no PW91 data available, the PBE parameters have also been used for this closely related functional.

For every carbon dioxide structure and every density functional used, relaxations of the atomic positions have been performed for a number of fixed volumes,[77] followed by a Levenberg–Marquardt least square fit[67] with the 3rd order Birch–Murnaghan equation of state (BM-EOS),[68]

$$\Delta E(V) = \Delta E(V_0) + \frac{9}{16} V_0 B_0 \left(\left[\left(\frac{V_0}{V} \right)^{\frac{2}{3}} - 1 \right]^3 B_0' + \left[\left(\frac{V_0}{V} \right)^{\frac{2}{3}} - 1 \right]^2 \left[6 - 4 \left(\frac{V_0}{V} \right)^{\frac{2}{3}} \right] \right), \quad (6)$$

with $\Delta E(V_0)$ being the energy difference taken for each phase i relative to the most stable phase I, and

$$\Delta E_i(V_0) = \frac{E_i(V_0)}{N_i} - \frac{E_0(\text{phaseI})}{N_{\text{phaseI}}}. \quad (7)$$

Here we note that the Helmholtz free energy A is identical with the internal energy $U(V) \approx E(V)$ at 0 K, and we used the first derivative to obtain the pressure as $p(V) = -\mathrm{d}E/\mathrm{d}V$. In addition, the BM-EOS provides information about the bulk modulus at zero pressure B_0, its first derivative with respect to the pressure, B_0', as well as the ground state volume V_0 at zero pressure. The index i refers to the respective phase/modification and ΔE_i denotes the energy difference between the most stable structure of phase i and the most stable structure of phase I, both at 0 GPa. N refers to the number of molecules in every cell in the usual crystallographic sense. From the $\Delta E_i(V_0)$ values of the crystal and the free molecule, we obtain the cohesive energy E_{coh} for each phase (zero point energy and temperature effects are neglected). Finally, the energy, pressure, and volume information can be used to calculate the enthalpy

$$H(V) = E + p(V) \cdot V \quad (8)$$

important for the discussion of thermodynamic phase stabilities with respect to the external pressure applied.

The experimental structures of phase III and phase VII are almost identical and the optimizations of the atomic positions in VASP resulted in the same ground state structures for 0 K. This is not surprising, since phase VII was found only for temperatures around 700 K[49] with a very similar structure as phase III at room temperature, whereas our calculations refer to 0 K. Therefore, the corresponding values are only listed once in the tables.

III. RESULTS AND DISCUSSION

A. Dispersion corrections

Figure 3 shows dispersion correction energies E_{disp} upon compression or decompression of the unit cells using the scaling factor λ_S, i.e.,

$$E_{\text{disp}}(V) \quad \text{with} \quad V = \lambda_S \cdot V_{\text{exp}}. \quad (9)$$

Here $\lambda_S = 1$ refers to the experimentally determined volumes V_{exp} from crystal structure measurements as listed in Table I.

Since the main contribution to the dispersive interactions is proportional to R_{AB}^{-6}, it increases for a compression and decreases upon decompression as clearly seen in Figure 3. The largest change occurs for the non-molecular structures, caused by the smaller interatomic distances in the initial cell volume in contrast to the more extended molecular phases. The usage of PBE-D3(ZD) instead of PBE-D2(ZD) results in a smaller value of E_{disp} for the non-molecular structures, while the usage of BJD increases the contribution for higher compression rates. Furthermore, the PBE-D3(BJD) method shows the most consistent (smooth) behavior with respect to the scaling factor λ_S for all phases.

The contribution of the long-range corrections to the ground state cohesive energy E_{coh} at 0 K and 0 GP is in all molecular cases very important and effects the values by more than 60% (absolute E_{coh} values can be found in Table II). Even though the dispersive part is dominant, the choice on the functional still has a large influence as will be discussed in Sec. III B.

B. Performance of the different density functionals

Table II shows that the cohesive energies for a specific phase can vary by as much as 25 kJ/mol between the different functionals, which is as high as the entire experimental enthalpy of sublimation at around 10^{-4} GPa.[8,9] The LDA

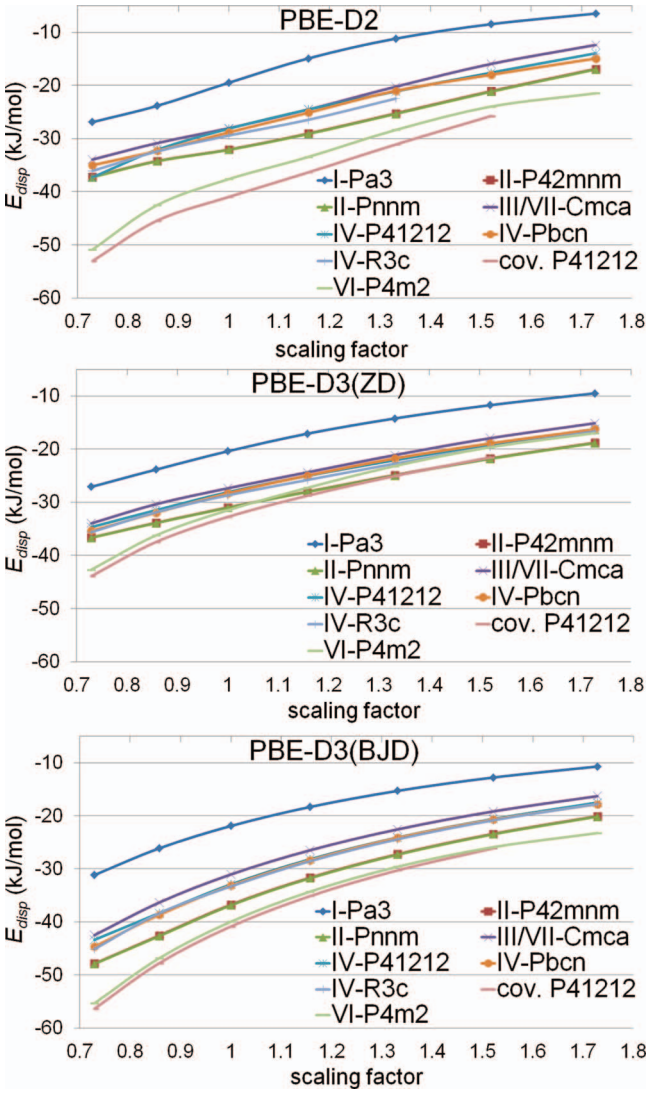

FIG. 3. Dispersion energy E_{disp} in kJ/mol with respect to the scaling factor λ_S according to Eq. (9). The x-axis shows the scaling factor λ_S, the y-axis refers to E_{disp}/N for a specific phase. The top figure was obtained with the PBE-D2 method, the middle one shows the results from the PBE-D3(ZD) method, and the results from the PBE-D3(BJD) method are shown in the bottom figure.

functional typically overbinds as one expects, thus largely underestimating the ground state volumes and overestimating the bulk moduli, and is therefore unsuitable to describe the molecular structures correctly, as can be seen in Table III. It therefore makes no sense to introduce a dispersion correction to LDA in the experimental pressure range. The two functionals PBE and PW91 give very similar results (with or without dispersion correction). The PBEsol version of PBE, where the parameters are adjusted to improve properties for condensed matter systems,[57] performs also reasonably well. The addition of the DFT-D correction improves the agreement of the bulk moduli with the experimental values but worsens the agreement for the volume significantly. On the other hand PBE-D2 gives the best result for the ground state volume at 1 GPa, while PBE-D3(BJD) and PBE-D3(ZD) provide bulk moduli closer to the experimental values. Similar findings have been obtained for the non-molecular phase V, as can be seen in

TABLE I. Experimental pressure p_{exp} (in GPa) and calculated values with the PBE-D3(BJD) functional: calculated volume at this pressure $V(p_{\text{exp}})$ (in Å^3), corresponding C–O distance (in Å) and O–C–O angle (in degrees). Furthermore, the volume at 0 GPa V_0 (in Å^3), bulk modulus B_0 (in GPa) with its pressure derivative B_0', and the cohesive energy E_{coh} at 0 GPa (in kJ/mol with respect to the free CO_2 molecule). Note that the experimental enthalpy of sublimation from Ref. 9 was measured for 760 mm hg ($\sim 10^{-4}$ GPa). Our calculated transition pressures p_{trans} (in GPa) are given with respect to phase I (molecular phases II, III, IV, and VII) or phase II (non-molecular modifications, including phases V and VI). For the I-$Pa\bar{3}$ phase, the CO distance at 0 GPa is $r_{\text{C-O}} = 1.168$ Å with a lattice constant of $a = 5.673$ Å. Values in curly brackets are from experimental data (except for Ref. 44, which are from molecular dynamic simulations). Cited references in the first column refer to the entire row if not stated otherwise. The experimental values in the III/VII-*Cmca* row refer to phase III (see text for further information). If available, the experimental values are given with their measurement uncertainties in round brackets. For Phase I-$Pa\bar{3}$, the X-ray diffraction pattern was solved with a R value of 0.041.[10] Phase IV-$R\bar{3}c$ was determined with a R value of 0.035.[14]

Phase	p_{exp}	$V(p_{\text{exp}})$	$r_{\text{C-O}}$	O–C–O	V_0	B_0	B_0'	E_{coh}	p_{trans}
I-$Pa\bar{3}$	1[10]	167.79 {165.85[10]}	1.168 {1.168[10]}	180 {180[10]}	182.62 {171.4(4)[33]}	9.4 {10.4(4)[33]}	5.5 {6.8(4)[33]}	−23.5 {−25.2[9]}	…
II-$P4_2/mnm$[37]	28	50.13 {51.72(1)}	1.157 {1.331(3)}	180 {180}	91.64	7.46 {131.5}	6.29 {2.1}	−21.15	7.53 {>10}
II-$Pnnm$[37]	28	50.14 {51.64(1)}	1.158 {1.331(3)}	180 {180}	91.58	7.50 {131.5}	6.28 {2.1}	−21.13	7.58 {>10}
III/VII-*Cmca*	11.8[48]	120.21 {120.24(5)[48]}	1.162 {1.16[48]}	180 {180[48]}	188.83	6.1 {87[37]}	6.9 {3.3[37]}	−21.6	14.6 {>11}
IV-$P4_12_12$[50]	15	117.72 {114.71(1)}	1.159 {1.5(1)}	179.84 {171.4(0)}	190.78	6.6	6.8	−19.3	… {>11}
IV-$Pbcn$[50]	15	114.94 {113.76(1)}	1.160 {1.5(1)}	178.41 {160.0(1)}	211.34	2.8	8.3	−18.5	… {>11}
IV−$R\bar{3}c$[14] (conv. cell)	15.2	790.59 {789.44(1)}	1.161 {1.155(2)}	180 {180}	1306.26	5.9	6.9	−21.6	11.1 {>11[50]}
V-$I\bar{4}2d$[41]	41	75.85 {74.68(1)}	1.368 {1.38(1)}	107.02 and 114.50 {106.6(2) and 115.4(5)}	92.82 {91.0(7)}	136.1 {136(11)}	4.0 {3.7(4)}	…	21.2 {∼ 40}
VI-$P\bar{4}m2$[44]	60	17.18 {17.36}	1.377 {1.381}	108.35 and 110.03 {108.64 and 109.89}	22.63	101.9	5.5	…	39.2 {∼50[46]}
$P4_12_12$[44]	80	67.63 {68.30}	1.334 and 1.353 {1.338 and 1.356}	107.19 and 108.63 {107.54 and 108.69}	92.00	128.8	4.5	…	26.3

TABLE II. Calculated cohesive energy values in kJ/mol for three exemplary molecular phases at 0 GPa, using different density functionals. For the experimentally derived cohesive energies see Table I.

Functionals	I-$Pa\bar{3}$	II-$P4_2/mnm$	IV-$R\bar{3}c$
LDA	− 34.7	− 30.2	− 30.9
PBE	− 8.7	− 5.8	− 6.1
PBEsol	− 9.0	− 5.8	− 7.2
PW91	− 13.1	− 10.1	− 10.5
PBE-D2	− 22.7	− 19.2	− 20.2
PBE-D3(BJD)	− 23.5	− 21.2	− 21.6
PBE-D3(ZD)	− 24.4	− 22.0	− 22.4
PBEsol-D3(BJD)	− 21.8	− 18.8	− 19.4
PW91-D3(BJD)	− 27.2	− 25.2	− 25.1

Table IV. Evaluating all calculated values, including cohesive energies and transition pressures, the PBE-D3(BJD) method gives perhaps the most consistent results compared to experimental values. Anyway, the results show that dispersion corrected density functionals give reasonable results for the solid-state properties of CO_2, further improvements towards accurate experimental values can only be obtained from methods which explicitly treat electron correlation within a many-body framework.[20,21]

C. Properties of the different CO_2 phases

Table I lists the experimental and theoretical properties of all investigated phases using the PBE-D3(BJD) functional. Concerning the discussion[32,36] about the correct structure of phase IV ($P4_12_12$, *Pbcn*, or $R\bar{3}c$), the tetragonal and orthorhombic structure solutions are predicted with higher cohesive energies (−19.3 and −18.5 kJ/mol, respectively) than the rhombohedral structure (−21.6 kJ/mol). While experiments suggested bond angles of less than 172° and 160° for the IV-$P4_12_12$ and IV-*Pbcn* solutions, respectively,[50] the angles always opened towards 180° (179.8° and 178.4°, respectively) in our computational structure optimization. Furthermore, the experimentally suggested, very long C–O bond distances of 1.5 Å were shortened to the length of C=O double bonds (about 1.16 Å for all three structural models), which is close to the experimentally found C–O bond length in IV-$R\bar{3}c$ of 1.155 Å.[14] All these findings are an indication for $R\bar{3}c$ being the best available structure solution of phase IV.

It is striking that the experimental bulk moduli for the strictly molecular phases II and III (131.5 and 87 GPa, respectively[37]) are almost as high as the 136 GPa for the non-molecular, covalent phase V.[38,41,69] Usually, molecular solid modifications are reported to have bulk moduli typically below 10 GPa,[31,32] and also other theoretical investigations[30,40] on these phases reported bulk moduli to be substantially lower and closer to our values of 7.46 GPa (II-$P4_2/mnm$), 7.50 GPa (II-*Pnnm*), and 6.1 GPa (III/VII-*Cmca*) than to the experimental ones. This leaves the experimentally reported bulk moduli for phase II and III questionable, especially since the experimental bulk modulus for phase I was reported to be around 10.4 GPa at 0 K,[33] which is close to our calculated value of 9.4 GPa. Other available experimental values can be found in Refs. 70 (8 GPa) and 37 (6.2 GPa). While Ref. 70 enables an estimation of the bulk modulus at 0 K from speed of sound measurements,[71] Ref. 37 does not provide information how the values where obtained and at what temperature. Nevertheless, all the experimental values for this strictly molecular phase I are below or close to 10 GPa, which supports the results of our calculations that bulk moduli above 100 GPa can be supported only for completely covalent carbon dioxide modifications as phase V-$I\bar{4}2d$ and phase VI-$P\bar{4}m2$.

Despite the other promising results of our investigations, we did not obtain meaningful differences for the two sug-

TABLE III. Results of the calculations for phase I-$Pa\bar{3}$ obtained for $p = 1$ GPa. All optimizations retained the local T_h symmetry and the experimental values are taken from Ref. 10 for 293 K and 1 GPa (V_0 from Ref. 33 and B_0 is stated separately in the table). Note that there are no information available how and at which conditions the bulk modulus in Ref. 37 has been obtained, while the other two cited bulk moduli refer to 0 K.

Property	Expt.	PBE	PBE-D2	PBE-D3(BJD)	PBE-D3(ZD)
$V(p)$ (Å^3)	165.85	183.12	165.33	167.79	169.05
a (Å)	5.494	5.679	5.489	5.515	5.529
r_{C-O} (Å)	1.168	1.168	1.168	1.168	1.168
O–C–O (deg)	180	180	180	180	180
V_0 (Å^3)	171.4(4)	217.34	176.25	182.62	183.30
B_0 (GPa)	10.4(4)[33]				
	8[71]	3.1	13.3	9.4	9.9
	6.2[37]				
B_0'	6.8(4)[33]	7.9	5.0	5.5	5.4
	6.1[37]				

Property	PW91	PW91-D3(BJD)	PBE_{sol}	PBE_{sol}-D3(BJD)	LDA
$V(p)$ (Å^3)	184.63	168.01	166.64	158.89	141.55
a (Å)	5.694	5.518	5.503	5.416	5.212
r_{C-O} (Å)	1.168	1.167	1.167	1.167	1.162
O–C–O (deg)	180	180	180	180	180
V_0 (Å^3)	234.85	184.78	188.87	176.14	152.90
B_0 (GPa)	1.3	8.0	5.2	6.8	8.4
B_0'	11.5	5.8	7.0	7.2	12.2

TABLE IV. Results of the calculations for phase V-$I\bar{4}2d$ with the PBE functional. The results are for $p = 41$ GPa and all optimizations retained the local D_{2d} symmetry. The experimental values are taken from Ref. 41 for 295 K and 41 GPa. Additional values are from Ref. 42 for room temperature and 43 GPa.

Property	Expt. 41 GPa[41]	Expt. 43 GPa[42]	PBE	PBE-D2	PBE-D3(BJD)	PBE-D3(ZD)
$V(p)$ (Å^3)	74.67(1)	74.69(1)	76.79	76.04	75.85	76.13
a (Å)	3.552(2)	3.5601(3)	3.599	3.582	3.583	3.586
c (Å)	5.919(3)	5.8931(9)	5.929	5.927	5.910	5.919
r_{C-O} (Å)	1.38(1)	1.353(2)	1.368	1.366	1.365	1.366
O–C–O (deg)	106.6(2)	107.2(1)	107.1	107.1	107.0	107.1
	115.4(5)	114.0(1)	116.8	114.3	114.5	114.4
V_0 (Å^3)	91.0(7)	...	94.22	92.64	92.82	92.95
B_0 (GPa)	136(11)	...	134.7	141.0	136.1	139.5
B_0'	3.7(4)	...	3.9	3.9	4.0	3.9

gested modifications of phase II—$P4_2/mnm$ (tetragonal) or $Pnnm$ (orthorhombic)—in order to be able to decide which structure solution might be the correct one. Differences in bond angles and bond distances are far too small, both experimentally and theoretically. This is also represented in the transition pressure, where the difference amounts to just 0.05 GPa, and the cohesive energies, which differ by only around 0.02 kJ/mol (cf. Table I). Small differences in the volume at 28 GPa (0.01 Å^3, $a = b = 3.51$, and $c = 4.06$ Å against $a = 3.47$, $b = 3.55$, and $c = 4.07$ Å) and the B_0 value (0.04 GPa) complete this picture and make it difficult to give a reliable statement on the most stable structure solution of phase II. The authors of Ref. 37 faced similar problems from their experimental measurement, and suggested therefore a tetragonal structure (II-$P4_2/mnm$) with orthorhombic distortion (II-$Pnnm$), which might be a plausible solution. But in contrast to the results of our calculations, Ref. 37 found the C=O bonds to be largely elongated, which was also challenged by DFT calculations from Bonev *et al.* Unfortunately, there is no other X-ray diffraction pattern available for this phase but as a result from our calculations, we would doubt these large C=O distances and suggest phase II to be strictly molecular, possibly within the $P4_2/mnm$ space group, since our optimized phase II structures show a convincing behavior on the relative enthalpies, as will be shown in Sec. III D.

D. Enthalpy and transition pressure

In order to access the most stable CO_2 modifications at any pressure as well as the transition pressures between two phases, Figure 4 shows a plot of all enthalpies with respect to the pressure. For simplification, the enthalpies are set relative to the enthalpy of phase I-$Pa\bar{3}$, i.e., the zero-line corresponds to phase I. The exact intersection values with phase I can be found in Table I as transition pressures p_{trans}. Comparing the transition pressures of phase IV-$P4_12_12$, -$Pbcn$, and -$R\bar{3}c$ with the phase diagram in Figure 1, only the $R\bar{3}c$ solution from Datchi and co-workers can be supported.

The predicted transition pressures for phases III/VII and IV-$R\bar{3}c$ are close to 12 GPa and therefore in excellent agreement with the experimental values. Especially for phase III, the experimental reports on the transition pressure are not very precise with a range between 11–13 GPa.[38,48,72–74] This was attributed to the strong kinetic effects in this region of the carbon dioxide phase diagram. Taking into account that phase II is thermodynamically stable and phase III only formed due to kinetic reasons, the (thermodynamic) transition pressure for phase II is in very good agreement with the experimental findings.

The predicted transition pressures for the non-molecular phases are not in such excellent agreement with the experimental values but still within an acceptable range. Interestingly, the $P4_12_12$ covalent crystal structure performs quite well in comparison to the phase V-$I\bar{4}2d$ and the theoretically proposed VI-$P\bar{4}m2$ structure. Even though it could not match the experimental diffraction patterns, this structure might still be a candidate in some other high-pressure region of the phase diagram. Temperature including calculations and/or further experiments will be necessary to allow for a further investigation of this structure.

Referring to Figure 4, the densities $\rho(p)$ (per CO_2 unit in the unit cell) for the most stable phases with respect to the pressure are shown in Figure 5. The thermodynamically predicted transition sequence is I-$Pa\bar{3}$ > II-$P4_2/mnm$ > V-$I\bar{4}2d$ for the PBE-D3(BJD) functional, which coincides with the order obtained from the standard PBE functional. Since our calculations did not include kinetic effects, only the thermodynamically stable phase II is represented between 10 and 20 GPa. A huge density rise is observed for the transition from the molecular modifications to the non-molecular phase V (around 0.8 g/cm^3), due to the now covalent CO_2 structure. The density rise between phases I and II is clearly smaller but nevertheless non-negligible (around 0.04 g/cm^3). Especially

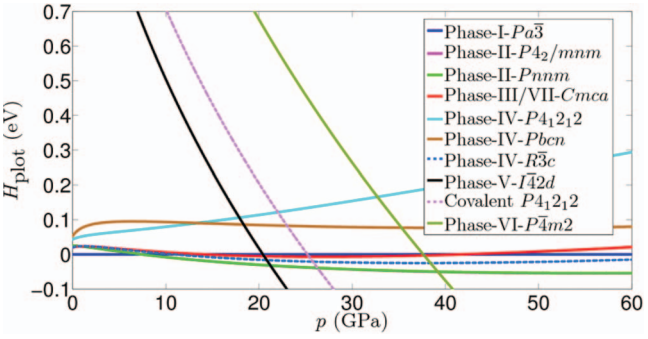

FIG. 4. Enthalpies for the investigated phases with respect to the enthalpy of phase I-$Pa\bar{3}$, using the PBE-D3(BJD) functional.

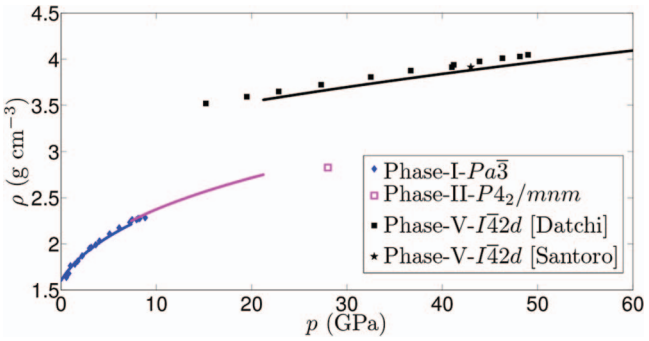

FIG. 5. Density (per CO_2 unit) of the most stable (according to our PBE-D3(BJD) calculations) carbon dioxide modifications with respect to the pressure. Markers show experimental values (I-$Pa\bar{3}$[33] (295 K values), II-$P4_2/mnm$,[50] II-$Pnnm$,[50] and V-$I\bar{4}2d$ from Datchi *et al.*[75] and Santoro *et al.*[42]), while the lines represent our calculated values. The most stable configurations are chosen according to Figure 4.

for phase I, the agreement with the experimental densities is excellent.

IV. SUMMARY

We performed first-principles DFT calculations on all known molecular solid modifications of carbon dioxide as well as on three non-molecular structures. Applying various DFT-D methods to account for weak van der Waals interactions improved the results significantly. Especially the PBE-D3(BJD) method is recommended for subsequent investigations.[76] Regarding the obtained transition pressures, cohesive energies, and ground state structures, the $R\bar{3}c$ modification described by Datchi and co-workers seems to be the best available solution for the structure of phase IV. The other two proposed structures featured largely elongated C=O distances. Together with the also elongated C=O distances in phase II, the authors of Refs. 37, 50 referred to them as intermediate modifications, while our investigations and also other theoretical and experimental results[14,30] find them to be strictly molecular. Moreover, the calculated bulk moduli for phases I and V are in very good agreement with the experimental findings, while the experimental values for phases II and III seem to be far too high for these molecular modifications.

Future investigations will have to include the calculations of temperature effects in order to access the high-temperature modifications of the molecular and especially the non-molecular carbon dioxide phases. In combination with further experimental investigations, this will hopefully lead to new insights into this largely unknown field of the phase diagram of carbon dioxide.

ACKNOWLEDGMENTS

We are grateful to D. Andrae, S. Biering, C. Müller, and A. Achazi for helpful discussions and suggestions, and to A. Punnett for outstanding technical support. Further, S. Gohr acknowledges financial support from the PROMOS program at the Freie Universität Berlin, and P.S. is indebted to the Alexander von Humboldt Foundation (Bonn) for financial support in terms of a Humboldt Research Award. The calculations have been performed on the high performance computing systems at the "Zentraleinrichtung für Datenverarbeitung - ZEDAT" (Freie Universität Berlin) and the "Marvin Compute Cluster" (Massey University Auckland).

[1]R. P. Stoffel, C. Wessel, M.-W. Lumey, and R. Dronskowski, Angew. Chem., Int. Ed. **49**, 5242 (2010).
[2]G. Maroulis, Chem. Phys. **291**, 81 (2003).
[3]N. J. Bridge and A. D. Buckingham, Proc. R. Soc. London, Ser. A **295**, 334 (1966).
[4]S. Coriani, A. Halkier, A. Rizzo, and K. Ruud, Chem. Phys. Lett. **326**, 269 (2000).
[5]Krishnaji and V. Prakash, Rev. Mod. Phys. **38**, 690 (1966).
[6]R. Bukowski, J. Sadlej, B. Jeziorski, P. Jankowski, K. Szalewicz, S. A. Kucharski, H. L. Williams, and B. M. Rice, J. Chem. Phys. **110**, 3785 (1999).
[7]A. Walsh, T. H. England, T. R. Dyke, and B. J. Howard, Chem. Phys. Lett. **142**, 265 (1987).
[8]J. S. Chickos and W. E. Acree, Jr., J. Phys. Chem. Ref. Data **31**, 537 (2002).
[9]W. F. Giauque and C. J. Egan, J. Chem. Phys. **5**, 45 (1937).
[10]R. T. Downs and M. S. Somayazulu, Acta Crystallogr., Sect. C: Cryst. Struct. Commun. **54**, 897 (1998).
[11]P. Schwerdtfeger and A. Hermann, Phys. Rev. B **80**, 064106 (2009).
[12]M. W. Mahoney and W. L. Jorgensen, J. Chem. Phys. **112**, 8910 (2000).
[13]A. Hermann and P. Schwerdtfeger, Phys. Rev. Lett. **101**, 183005 (2008).
[14]F. Datchi, V. M. Giordano, P. Munsch, and A. M. Saitta, Phys. Rev. Lett. **103**, 185701 (2009).
[15]C. S. Yoo, A. Sengupta, and M. Kim, Angew. Chem., Int. Ed. **50**, 11219 (2011).
[16]C. Müller and B. Paulus, Phys. Chem. Chem. Phys. **14**, 7605 (2012).
[17]G. H. Booth, A. Grüneis, G. Kresse, and A. Alavi, Nature (London) **493**, 365 (2012).
[18]M. A. Morales, C. Pierleoni, and D. M. Ceperley, Phys. Rev. E **81**, 021202 (2010).
[19]D. M. Ceperley, Rev. Mod. Phys. **67**, 279 (1995).
[20]J. Harl and G. Kresse, Phys. Rev. Lett. **103**, 056401 (2009).
[21]B. Paulus, Phys. Rep. **428**, 1 (2006).
[22]B. G. Janesko, T. M. Henderson, and G. E. Scuseria, Phys. Chem. Chem. Phys. **11**, 443 (2009).
[23]J. Klimeš and A. Michaelides, J. Chem. Phys. **137**, 120901 (2012).
[24]S. Grimme, J. Antony, S. Ehrlich, and H. Krieg, J. Chem. Phys. **132**, 154104 (2010).
[25]W. Hujo and S. Grimme, Phys. Chem. Chem. Phys. **13**, 13942 (2011).
[26]R. Podeszwa and K. Szalewicz, J. Chem. Phys. **136**, 161102 (2012).
[27]O. A. Vydrov and T. V. Voorhis, J. Chem. Theory Comput. **8**, 1929 (2012).
[28]T. Risthaus and S. Grimme, J. Chem. Theory Comput. **9**, 1580 (2013).
[29]Z. Chang, D.-S. Zhang, Q. Chen, and X.-H. Bu, Phys. Chem. Chem. Phys. **15**, 5430 (2013).
[30]S. A. Bonev, F. Gygi, T. Ogitsu, and G. Galli, Phys. Rev. Lett. **91**, 065501 (2003).
[31]M. Santoro and F. A. Gorelli, Chem. Soc. Rev. **35**, 918 (2006).
[32]C.-S. Yoo, Phys. Chem. Chem. Phys. **15**, 7949 (2013).
[33]V. M. Giordano, F. Datchi, F. A. Gorelli, and R. Bini, J. Chem. Phys. **133**, 144501 (2010).
[34]A. Sengupta and C.-S. Yoo, Phys. Rev. B **80**, 014118 (2009).
[35]A. Sengupta and C.-S. Yoo, Phys. Rev. B **82**, 012105 (2010).
[36]C.-S. Yoo, A. Sengupta, and M. Kim, High Press. Res. **31**, 68 (2011).
[37]C.-S. Yoo, H. Kohlmann, H. Cynn, M. F. Nicol, V. Iota, and T. LeBihan, Phys. Rev. B **65**, 104103 (2002).
[38]C.-S. Yoo, H. Cynn, F. Gygi, G. Galli, V. Iota, M. Nicol, S. Carlson, D. Häusermann, and C. Mailhiot, Phys. Rev. Lett. **83**, 5527 (1999).
[39]J. Dong, J. K. Tomfohr, O. F. Sankey, K. Leinenweber, M. Somayazalu, and P. F. McMillan, Phys. Rev. B **62**, 14685 (2000).
[40]L. Gracia, M. Marques, A. Beltran, A. M. Pendas, and J. M. Recio, J. Phys.: Condens. Matter **16**, S1263 (2004).
[41]F. Datchi, B. Mallick, A. Salamat, and S. Ninet, Phys. Rev. Lett. **108**, 125701 (2012).
[42]M. Santoro, F. A. Gorelli, R. Bini, J. Haines, O. Cambon, C. Levelut, J. A. Montoya, and S. Scandolo, Proc. Natl. Acad. Sci. U.S.A. **109**, 5176 (2012).
[43]A. Togo, F. Oba, and I. Tanaka, Phys. Rev. B **77**, 184101 (2008).
[44]J. Sun, D. D. Klug, R. Martonak, J. A. Montoya, M.-S. Lee, S. Scandolo, and E. Tosatti, Proc. Natl. Acad. Sci. U.S.A. **106**, 6077 (2009).

[45]M.-S. Lee, J. A. Montoya, and S. Scandolo, Phys. Rev. B **79**, 144102 (2009).
[46]V. Iota, C.-S. Yoo, J.-H. Klepeis, Z. Jenei, W. Evans, and H. Cynn, Nature Mater. **6**, 34 (2007).
[47]S. N. Steinmann and C. Corminboeuf, J. Chem. Theory Comput. **7**, 3567 (2011).
[48]K. Aoki, H. Yamawaki, M. Sakashita, Y. Gotoh, and K. Takemura, Science **263**, 356 (1994).
[49]V. M. Giordano and F. Datchi, EPL **77**, 46002 (2007).
[50]J.-H. Park, C.-S. Yoo, V. Iota, H. Cynn, M. F. Nicol, and T. Le Bihan, Phys. Rev. B **68**, 014107 (2003).
[51]S. H. Vosko, L. Wilk, and M. Nusair, Can. J. Phys. **58**, 1200 (1980).
[52]D. M. Ceperley and B. J. Alder, Phys. Rev. Lett. **45**, 566 (1980).
[53]J. P. Perdew, K. Burke, and M. Ernzerhof, Phys. Rev. Lett. **77**, 3865 (1996).
[54]J. P. Perdew, K. Burke, and M. Ernzerhof, Phys. Rev. Lett. **78**, 1396 (1997).
[55]J. P. Perdew, J. A. Chevary, S. H. Vosko, K. A. Jackson, M. R. Pederson, D. J. Singh, and C. Fiolhais, Phys. Rev. B **46**, 6671 (1992).
[56]J. P. Perdew, J. A. Chevary, S. H. Vosko, K. A. Jackson, M. R. Pederson, D. J. Singh, and C. Fiolhais, Phys. Rev. B **48**, 4978 (1993).
[57]J. P. Perdew, A. Ruzsinszky, G. I. Csonka, O. A. Vydrov, G. E. Scuseria, L. A. Constantin, X. Zhou, and K. Burke, Phys. Rev. Lett. **100**, 136406 (2008).
[58]G. Kresse and J. Hafner, Phys. Rev. B **47**, 558 (1993).
[59]G. Kresse and J. Hafner, Phys. Rev. B **49**, 14251 (1994).
[60]G. Kresse and J. Furthmüller, Phys. Rev. B **54**, 11169 (1996).
[61]G. Kresse and J. Furthmüller, Comput. Mater. Sci. **6**, 15 (1996).
[62]P. E. Blöchl, Phys. Rev. B **50**, 17953 (1994).
[63]G. Kresse and D. Joubert, Phys. Rev. B **59**, 1758 (1999).
[64]S. Grimme, J. Comput. Chem. **27**, 1787 (2006).
[65]S. Grimme, S. Ehrlich, and L. Goerigk, J. Comput. Chem. **32**, 1456 (2011).
[66]See http://www.thch.uni-bonn.de/tc/?section=downloadslang=english for the program.
[67]J. W. Eaton, *GNU Octave Manual* (Network Theory Limited, 2002).
[68]F. Birch, Phys. Rev. **71**, 809 (1947).
[69]Y. Seto, D. Nishio-Hamane, T. Nagai, N. Sata, and K. Fujino, J. Phys.: Conf. Ser. **215**, 012015 (2010).
[70]V. G. Manzhelii, A. M. Tolkachev, M. I. Bagatskii, and E. I. Voitovich, Phys. Status Solidi **44**, 39 (1971).
[71]Bulk modulus B_0 extracted from Fig. 6 and Eq. (15) in Ref. 70.
[72]V. Iota and C.-S. Yoo, Phys. Rev. Lett. **86**, 5922 (2001).
[73]M. Santoro, J. Lin, H. Mao, and R. J. Hemley, J. Chem. Phys. **121**, 2780 (2004).
[74]H. Olijnyk and A. P. Jephcoat, Phys. Rev. B **57**, 879 (1998).
[75]F. Datchi, private communication (September 2013), values at 295 K.
[76]J. G. Brandenburg and S. Grimme, Theor. Chem. Acc. **132**, 1399 (2013).
[77]See supplementary material at http://dx.doi.org/10.1063/1.4826929 for the raw data values (volume, pressure, total energy, and dispersion energy) extracted from the VASP optimizations at defined volumes.